Accepted Manuscript

Synthesis of naphthazarin derivatives and identification of novel thioredoxin reductase inhibitor as potential anticancer agent

Junmin Zhang, Yaping Liu, Danfeng Shi, Guodong Hu, Baoxin Zhang, Xinming Li, Ruijuan Liu, Xiao Han, Xiaojun Yao, Jianguo Fang

PII: S0223-5234(17)30741-9

DOI: 10.1016/j.ejmech.2017.09.027

Reference: EJMECH 9742

To appear in: *European Journal of Medicinal Chemistry*

Received Date: 3 April 2017

Revised Date: 15 September 2017

Accepted Date: 15 September 2017

Please cite this article as: J. Zhang, Y. Liu, D. Shi, G. Hu, B. Zhang, X. Li, R. Liu, X. Han, X. Yao, J. Fang, Synthesis of naphthazarin derivatives and identification of novel thioredoxin reductase inhibitor as potential anticancer agent, *European Journal of Medicinal Chemistry* (2017), doi: 10.1016/j.ejmech.2017.09.027.

This is a PDF file of an unedited manuscript that has been accepted for publication. As a service to our customers we are providing this early version of the manuscript. The manuscript will undergo copyediting, typesetting, and review of the resulting proof before it is published in its final form. Please note that during the production process errors may be discovered which could affect the content, and all legal disclaimers that apply to the journal pertain.

Graphical abstract

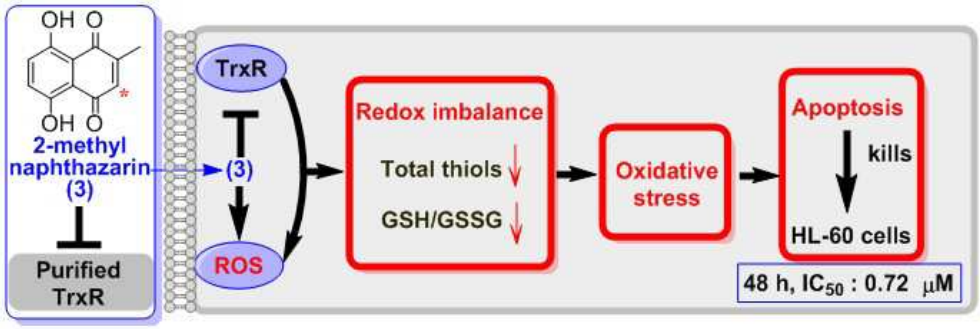

ACCEPTED MANUSCRIPT

ACCEPTED MANUSCRIPT

Synthesis of naphthazarin derivatives and identification of novel thioredoxin reductase inhibitor as potential anticancer agent

Junmin Zhang [a, b, c], Yaping Liu [a, c], Danfeng Shi [c], Guodong Hu [a, c], Baoxin Zhang [a, c], Xinming Li [a, c], Ruijuan Liu [a, b], Xiao Han [a, c], Xiaojun Yao [c] and Jianguo Fang [a, c]*

[a] *State Key Laboratory of Applied Organic Chemistry,* [b] *School of Pharmacy, and* [c] *College of Chemistry and Chemical Engineering, Lanzhou University, Lanzhou, Gansu 730000, China*

* Corresponding author. Tel: +86 931 8912500; fax: +86 931 8915557.

E-mail: fangjg@lzu.edu.cn (J. Fang).

ACCEPTED MANUSCRIPT

ACCEPTED MANUSCRIPT

Abstract

Mammalian thioredoxin reductase (TrxR) enzymes play a crucial role in regulating multiple redox-based signaling pathways and have attracted increasing attention as promising anticancer drug targets. We report here the synthesis of a panel of naphthazarin derivatives and discovery of 2-methyl-5,8-dihydroxy-1,4-naphthoquinone (**3**, 2-methylnaphthazarin) as a potent cytotoxic agent with a submicromolar half maximal inhibitory concentration to the human promyelocytic leukemia HL-60 cells. Mechanism studies reveal that the compound selectively inhibits TrxR to induce oxidative stress-mediated apoptosis of HL-60 cells. Knockdown of TrxR sensitizes the cells to **3** insults, while overexpression of the functional enzyme confers resistance to the compound treatment, underpinning the physiological significance of targeting TrxR by **3**. Clarification of the interaction of compound **3** with TrxR unveils the cellular action of the compound, and sheds light in considering development of the compound as a potential cancer chemotherapeutic agent.

Keywords: Naphthazarin derivatives; 2-methylnaphthazarin; Thioredoxin reductase; Reactive oxygen species; Oxidative stress; Apoptosis.

***Abbreviations*:** BSO: L-buthionine-(S,R)-sulfoximine; DCFH-DA: 2', 7'-dichlorfluorescein diacetate; DHE: dihydroethidium; GR: glutathione reductase; HeLa-shTrxR1: HeLa cells transfected with shTrxR1 plasmids; HeLa-shNT: HeLa cells transfected with shNT plasmid; HEK-TrxR1: HEK 293T cells stably overexpressing TrxR1; HEK-IRES: HEK 293T cells stably transfected with a vector; NAC: N-acetyl-L-cysteine; ROS: reactive oxygen species; Sec: selenocysteine; Trx: thioredoxin; TrxR: thioredoxin reductase.

1. Introduction

The thioredoxin system, consisting of NADPH, thioredoxin reductase (TrxR) and thioredoxin (Trx), is a major disulfide reductase system that transfers electrons from NADPH to a multitude of enzymes, and plays an essential role in regulating multiple cellular redox signaling pathways [1-3]. Elevated levels of Trx/TrxR are frequently observed in different types of cancer, and are recognized as association with aggressive cancers, poor patient prognosis and resistance to chemotherapy [4, 5]. Furthermore, transfection with dominant-negative mutant Trx or depletion of TrxR results in a retardation in tumor progression and metastasis [6, 7]. Accordingly, the thioredoxin system has been a promising target for anticancer drug development [1, 8]. The past decades have witnessed growing interests in identifying and developing small molecules targeting the TrxR/Trx as potential cancer chemotherapeutic agents [8-16].

The diversity of natural products such as quinones, flavonoids, terpenoids, and alkaloids has inspired the drug discovery, and is still a unique source of biologically active lead compounds [17, 18]. Approximately, half of the drugs in the market are natural products or their derivatives. In the case of anti-infective and anticancer agents, this ratio is even higher [19]. As an essence of the drug discovery progress, the generation of novel and structurally diverse lead compounds with potential pharmacological properties has been actively sought. Among these natural products, 1, 4-naphthoquinones are an important family. The 1,4-naphthoquinone pharmacophore is known to afford antitumor activity in a number of clinically used drugs, such as streptonigrin [20], mitomycins [21], and doxorubicin [22]. Naphthazarin (5, 8-dihydroxy-l, 4-naphthoquinone) is one of a natural 1, 4-naphthoquinone derivatives derived from the roots of several members of the genus *Boraginaceae* [23] and is employed in food, cosmetics and textiles. Naphthazarin derivatives have been documented possessing a wide variety of pharmacological activities due to containing a 1, 4-naphthoquinone pharmacophore, including antiinflammatory, anticancer, antibacterial, antioxidant, and antifungal effects [24-27]. Ahn *et al.* synthesized a series of naphthazarin derivatives through modifying 5, 8-dihydroxy, and evaluated their cytotoxicity and inhibition of DNA topoisomerase I [28-30]. In recent years, large attention has been paid to the potential anticancer potency of naphthazarin derivatives due to induction of apoptosis in multiple types of tumor cells, and various putative cellular mechanisms were proposed, including oxidative stress [24], depolymerization of microtubules [25], interference with lysosomal function [31], activation of mitochondrial apoptosis

inducing factor (AIF) [32] and p53-dependent p21 activation [33]. Shikonin, a naturally occurring naphthazarin derivative, was previously investigated for killing cancer cells *via* targeting TrxR by our lab [15]. In consideration of the importance of 5, 8-dihydroxy-l, 4-naphthoquinone scaffold, we synthesized a series of 2-substituted naphthazarin derivatives, and evaluated their cytotoxicity in a panel of tumor cells and normal cells. After initial cytotoxicity screening, we discovered that **3** (2-methylnaphthazarin) displayed the most cytotoxic effect against HL-60 cells with an IC_{50} value of 0.72 μM after 48 h treatment. The follow-up studies disclosed that **3** results in a time- and concentration-dependent inhibition of the TrxR. The pharmacological action of **3** in cells involves inhibition of TrxR, accumulation of reactive oxygen species (ROS), decrease of GSH/GSSG ration and cellular total thiols, and activation of caspase 3. Finally, compound **3** elicits oxidative stress-mediated apoptosis of HL-60 cells. Knockdown of TrxR sensitizes the cells to **3** insults, while overexpression of the functional enzyme alleviates the cytotoxicity, underpinning the physiological significance of targeting TrxR by **3**. We expect that **3** could be a novel cancer chemotherapeutic agent for further development.

2. Results

2.1. Chemistry

Synthesis of the naphthoquinone derivatives was performed by condensation of maleic anhydrides with various phenols under a molten mixture of aluminium chloride and sodium chloride [34]. The general synthetic routes were depicted in Scheme 1. After construction of the naphthazarin (**2**) scaffold, various substituted naphthazarin were prepared *via* reactions of **2** with different amines in ethanol as described in the literatures [35, 36]. The resulting products were purified by silica gel column chromatography. All the naphthoquinone derivatives were fully characterized by ^{1}H, ^{13}C NMR, and mass spectrometry. The original NMR spectra of compounds were shown in the Supporting Information (Fig. S1-S30).

2.2. Evaluation of cytotoxicity.

Initially, we employed the MTT assay to assess the cytotoxicity of all the synthetic compounds (**1-16**, structures presented in Scheme 1 and Table 1) towards HL-60 cells at a fixed concentration of 20 μM over a duration of 48 h. Under this condition, the cell viability was summarized and listed in

Table 1. Compounds **2** and **3** showed the highest cytotoxicity. Analyzing the cytotoxicity data reveals that introducing a substituted amino group to the quinone double bond (compounds **4**-**16**) significantly decreases the cytotoxicity, which provides information for further preparation of such compounds. Next, we chose these two compounds for the follow-up studies. As shown in Fig.1A, compounds **2** and **3** display comparable efficacy toward HL-60 tumor cells with a submicromolar IC_{50} value after 48 or 72 h treatment, but compound **3** appears higher potency. As compounds **2** and **3** have similar structures, it is likely that they share the same action mechanism in cells. Thus, we chose **3** to confirm the results from the MTT assay by employing the trypan blue exclusion assay, which gives an IC_{50} value of 0.86 μM (Fig. 1C) upon treatment of HL-60 cells for 48 h. This is quite consistent with the value from the MTT assay (IC_{50}=0.72 μM). To confirm whether **3** is cytotoxic to other tumor cells and normal cells, several human cancer and noncancerous cell lines were treated with various concentrations of **3** for 48 h, including human alveolar adenocarcinoma cell line A549, human cervical cancer cell line HeLa, human hepatocellular carcinoma cell line HepG2, human embryonic kidney 293T cell line HEK 293T and human immortalized normal liver cell line L02. As shown in Fig. 1B, compound **3** exhibited the most potency on HL-60 cells compared with other cell types. Interestingly, compound **3** displays less potency to L02 cells and HEK 293T cells, two noncancerous cell lines (Fig. 1D). Collectively, our results demonstrate that compound **3** possesses the promising cytotoxicity in all compounds and inhibits growth of multiple cell lines, with the most potency to HL-60 cells. Thus, our follow-up studies were focused on **3**.

*2.3. Inhibition of TrxR by **3** in vitro*

Since **3** displays the highest cytotoxicity to HL-60 cells, we then asked the possible cellular target of the compound. Compound **3** belongs to the naphthoquinone family, a class of reactive natural products whose chemical structures allow them to interact with pharmacological targets by forming covalent bonds and/or by serving on electron transfer agents in biological redox reactions [37]. More importantly, its structure is reminiscent of shikonin [15], and juglone [38], two established TrxR inhibitors. Thus we speculated that **3** might be a novel inhibitor of TrxR. Initially, we determined whether compound **3** inhibits TrxR using the purified enzyme. Incubation of **3** with the reduced enzyme causes a dose-dependent inhibition of its activity with an IC_{50} value around 0.7 μM (Fig. 2A), which is more potent than other known TrxR inhibitors, such as securinine [14],

shikonin [15], and parthenolide [16] . Removal of **3** from the incubation mixture by desalting column did not recover the enzyme activity, suggesting compound **3** inhibits TrxR1 irreversibly. TrxR possess an N-terminal redox center characterized by a dithiol motif (-Cys-XXXX-Cys-) and a C-terminal active site with a -Cys-Sec- motif. The Sec residue has a significantly low pKa value (5.24 for the selenol/selenate couple compared to 8.25 for the thiol/thiolate couple), resulting in an enhanced nucleophilic property [39, 40]. As many TrxR inhibitors have been demonstrated to target the Sec residue in the enzyme [11, 13, 14, 41], next, we determined whether **3** also targets the Sec residue by comparing the inhibition potency of **3** towards the wild type enzyme and the mutant U498C TrxR enzyme, where the Sec498 was replaced by Cys. As shown in Fig. 2A, compound **3** gave very weak inhibition to U498C TrxR. Glutathione reductase (GR) is a homologous of TrxR with a similar overall structure but lacks the C-terminal -Cys-Sec- redox center. Compound **3** had marginal effect on the enzyme activity (Fig. 2A). Selectively inhibiting WT enzyme but not U498C TrxR or GR implies the Sec residue is specifically targeted by **3**. In addition, the possible binding mode for compound **3** with TrxR protein was figured out by the covalent docking method. As shown in Fig. 2B, the carbon atom indicated with an asterisk of compound **3** connects covalently with the selenium atom of Sec498. The binding pocket for compound **3** was formed by the C-terminal active site redox center of one subunit constituted by Gly496, Cys497, Sec498, Gly499 and some hydrophobic residues of the other subunit including Val60', Ile65', Leu112', Ile347'. A hydrogen bonding was found between the phenolic hydroxyl group of compound **3** and the carboxyl group of Gly499 and a π-π stacking interaction also occurs between the benzene ring of compound **3** and the imidazolyl group of His472. All these results presented a clear view that compound **3** reacts with Sec498 of TrxR irreversibly by forming a covalent bond and all the non-bonding interactions between compound **3** and the residues around Sec498 seems to supply a favorable environment for the formation of the covalent bond. Taken together, compound **3** selectively targets the Sec residue in TrxR to inhibit its activity *in vitro*.

*2.4. Inhibition of TrxR contributes to the cytotoxicity of **3***

Since compound **3** effectively inhibits the purified TrxR, to extend this discovery in a cellular content, we determined the inhibition of TrxR in HL-60 cells. Firstly, we employed the TRFS-green, a specific TrxR fluorescence probe developed by our lab [42], to assess the cellular TrxR activity. As

illustrated in Fig. 3A, treatment of HL-60 cells with **3** causes a dose-dependent decrease of the fluorescence, demonstrating the inhibition of TrxR by **3**. Secondly, we performed the classic Trx-mediated insulin reduction assay to confirm the fluorescence results. Again, treatment of HL-60 cells with **3** causes a remarkable decrease in the cellular TrxR activity with an IC_{50} value around 2.4 μM (Fig. 3B), which is more potent than other known TrxR inhibitors, such as securinine [14], parthenolide [16], and alantolactone [41]. There appears no apparent change of TrxR1 expression after the HL-60 cells were treated with **3** for 24 h (Fig. 3C), suggesting that the decreased enzyme activity is caused by the direct inhibition of TrxR. Finally, to further demonstrate whether the inhibition of TrxR is involved in the cytotoxicity of **3**, we then turned to compare the sensitivity of the cells that stably transfected with a vector (HEK-IRES) and HEK cells stably overexpressing TrxR1 (HEK-TrxR1) towards **3** treatment. The transfection efficiency was confirmed by measuring the enzyme activity and the protein expression in our previous publication [41]. As shown in Fig. 3D, **3** shows lower cytotoxicity to HEK-TrxR1 cells than HEK-IRES cells. Meanwhile, to further verify the biological relevance of TrxR-mediated cytotoxicity of **3**, we further determined the cytotoxicity of 3 after knocking down TrxR expression. Due to the low transfection efficiency of HL-60 cells, we employed the HeLa cells for the knockdown experiments. Knockdown of TrxR1 in HeLa cells (HeLa-shTrxR1) was assessed in our group previous publication [41]. TrxR knockdown could yield drug-specific alteration of cytotoxicity of small molecule drugs [43]. We observed that **3** displays elevated potency to HeLa-shTrxR1 cells compared with the cells only transfected with a non-targeting vector (HeLa-shNT) (Fig. 3E). Taken together, our results revealed that inhibition of TrxR is involved in the cellular action of **3**.

*2.5. Induction of oxidative stress by **3** in HL-60 cells*

The thioredoxin system is critical for the intracellular redox balance to prevent excess ROS accumulation. A great majority of TrxR inhibitors, such as curcumin [44] and shikonin [15], could promote ROS production and induce oxidative stress. Accordingly, we determined whether compound **3** has the similar effects. Firstly, DCFH-DA was employed to assess the overall ROS levels in HL-60 cells. DCFH-DA is a well-established probe to determine intracellular levels of ROS. As shown in Fig. 4A, the ROS levels in HL-60 cells are undetectable under basal conditions. Treatment of the HL-60 cells with **3** notably promotes the ROS production. The higher concentration

of **3** leads to more ROS generation. The DCFH-DA-based ROS assay is prone to artifacts as extensively discussed in the literature [45], we further employed another probe, DHE, to confirm the ROS generation in HL-60 cells. Again, compound **3** evokes the fluorescence in a dose-dependent manner (Fig. 4B). Collectively, these data indicated that **3** could promote ROS accumulation in HL-60 cells.

Cellular thiols are important antioxidants to neutralize ROS accumulation. To assess the overall redox states of the HL-60 cells after **3**-treatment, the amount of thiols was determined by DTNB titration. After HL-60 cells were treated with **3**, the amount of cellular thiols is decreased (Fig. 4C). Furthermore, we assessed the changes of glutathione homeostasis in HL-60 cells treated with the indicated concentration of **3**. As shown in Fig. 4D, incubation of **3** with the cells causes a reduction of the ratio of GSH/GSSG dose-dependently. Accumulation of ROS and oxidation of thiols indicate the intracellular environment is shifted to an oxidative state. Thus, we further asked if the additional oxidative stimulants could improve the cytotoxicity of **3**. As shown in Fig. 4E, pretreatment of the HL-60 cells with **3** significantly incited the cells to hydrogen peroxide challenge. Under our experimental conditions, hydrogen peroxide (50 μM) and **3** (1 μM) caused 4% and 27% cell death, respectively. However, treatment with a combination of hydrogen peroxide and **3** stimulates more than 43% cell death, indicating that **3** has synergistic action with hydrogen peroxide to induce cell death. A similar effect was observed for the combination of 3 μM of **3** with hydrogen peroxide. Taken together, all these data support the induction of oxidative stress by **3** in HL-60 cells.

2.6. Promotion of cell death by GSH depletion and protection of cell death by NAC

As **3** could lead to disorder of cellular redox balance and induction of oxidative stress in HL-60 cells, we next explored the functions of GSH depletion and NAC supplement in the process of **3**-induced HL-60 cell death. NAC is a thiol antioxidant and precursor for biosynthesis of GSH. Pretreatment of the HL-60 cells with NAC alleviates the cytotoxicity of **3**, and a high concentration of NAC (5 mM) completely rescues the cells (Fig. 5A). Next, we measured the effect of GSH depletion on the cytotoxicity of **3**. In contrast to the protective role of NAC, depletion of the cellular GSH by pretreatment of the cells with BSO remarkably augments the cytotoxicity of **3** (Fig. 5B). Under our experimental conditions, the intracellular GSH level was reduced to less than 20% of the control after treatment of HL-60 cells with 50 μM BSO for 24 h. GSH is a crucial component of

glutathione system, another redox regulation network besides thioredoxin system in cells. Our results that depletion of cellular GSH sensitizes the cytotoxicity while supplement of NAC protects the cells to **3** treatment support the oxidative stress is engaged in the pharmacological action of **3**.

2.7. Induction of apoptosis in HL-60 cells

We presented evidence here that **3** kills HL-60 cells predominantly through the induction of apoptosis (Fig. 6). Since the apoptotic process is an early event of cell death, we chose a shorter treatment time (24 h) for the apoptosis assay. It is well known that caspase 3 is a major component of apoptotic machinery in mammalian cells, and its activation is one of hallmarks in the process of apoptosis. We detected the activation of caspase 3 after **3** treatment. As shown in Fig. 6A, compound **3** activates caspase 3 activity in HL-60 cells. However, a higher concentration of **3** (5 μM) decreased the activity of caspase 3 slightly. This could be due to inactivation of caspase 3 by the high concentration of **3.** When HL-60 cells were incubated with indicated concentrations of **3** followed by Hoechst 33342 staining, an increasing number of cells exhibited condensed and highly fluorescent nuclei, a characteristic morphology of cells undergoing apoptosis (Fig. 6B). Further evidence from the Annexin V-FITC/PI double staining assay quantified the apoptotic population by flow cytometer (Fig. 6 C&D). Treatment of the cells with 0.5 μM, 1 μM, 3 μM and 5 μM **3** for 24 h causes ~10%, ~23%, ~42% and ~56% cell apoptosis, respectively. Again, NAC could antagonize the apoptosis. A slight increase of the necrotic cells was observed after the cells were treated with 5 μM **3** for 24 h, consistent with the higher concentration of **3** (5 μM) decrease the activation of caspase 3 (Fig. 6A). This could be due to the excessive oxidative stress caused by **3**. Taken together, our results reveal that compound **3** predominantly induces apoptosis in HL-60 cells.

3. Discussion

l, 4-Naphthoquinone moiety is believed to be an essential pharmacophore of many pharmaceutically active compounds. We have synthesized a series of 2-substituted l, 4-naphthoquinone derivatives, evaluated their anticancer activity, and explored the underlying mechanism. Among these compounds, compound **3** inhibits the growth of multiple cell lines, with the most potency to HL-60 cells. We presented evidence herein that the cytotoxicity of **3** is mediated, at least in part, by targeting the selenoenzyme TrxR. Firstly, we compared the inhibition potency of **3**

to the purified WT TrxR1, GR and U498C TrxR1 (Fig. 2A). Single mutation of Sec to Cys sharply decreased the potency of **3**, suggesting that the Sec residue in TrxR is a primary target of **3**. The structure of GR is closely related to TrxR, however, under our experimental conditions, very weak inhibition of GR was observed. The selective inhibition of WT TrxR1 but not U498C TrxR1 nor GR suggests a specific interaction of **3** with TrxR. Secondly, we also investigated the binding mode of compound **3** with TrxR using the covalent docking method (Fig. 2B), supporting the covalent bond formation between Sec498 and compound **3**. Binding of **3** to the enzyme is further supported by a series of non-bonding interactions between the compound and the residues around Sec498. Thirdly, we provided evidence in cellular contexts to support the unique role of TrxR for the cellular action of **3**. Compound **3** displays remarkable inhibition of TrxR activity in intact cells and in cell lysates (Fig. 3A & B). More importantly, involvement of TrxR inhibition to the cytotoxicity by **3** was further demonstrated by the TrxR overexpression and knockdown experiments (Fig. 3D & E). Under our experimental conditions, compound **3** displays potent cytotoxicity to a variety of cancer cells, but has the highest potency to HL-60 cells (Fig. 1B). We reasoned this selectivity may be related to the intrinsic TrxR activity in different cells. HL-60 cells, which are most sensitive to **3** among the four tested cell lines, show the lowest TrxR activity [15]. TrxR knockdown experiments further confirm this result (Fig. 3 E). Finally, the glutathione system and thioredoxin system are two major networks. Although they work independently, a few crosstalks enable them acting as mutual backup in managing the intracellular redox homeostasis [46]. Our observations that depletion of cellular GSH by BSO elevates the cytotoxicity, while upregulation of GSH by NAC lessens the cytotoxicity of **3** (Fig. 5A & B) also suggest that TrxR is involved in the cellular action of **3**. Inhibition of TrxR would further promote accumulation of ROS, decrease cellular thiol pool, and finally elicit oxidative stress.

Acquiring resistance toward apoptosis is one of the hallmarks of malignant cells [47]. Activation of apoptosis in tumor cells is thus indispensable to tumor therapy. We provided evidence that the cell death caused by **3** is predominantly through apoptosis (Fig. 6), thereby strengthening the application of **3** in treatment of cancer. In addition, as we have demonstrated that treatment of the cells with **3** promotes accumulation of ROS, decrease of GSH/GSSG ration and depletion of intracellular total thiols in HL-60 cells, it is most likely that **3** induces oxidative stress-mediated apoptosis. Based on these results shown, we here presented that targeting TrxR by **3** contributes to inducing oxidative stress-mediated apoptosis of HL-60 cells.

In summary, we have synthesized a series of l, 4-naphthoquinone derivatives and discovered compound **3** as a potent cytotoxic agent with a submicromolar half maximal inhibitory concentration to HL-60 cells. The follow-up mechanistic studies disclosed that the cellular action of compound **3** is related to its ability to target the selenoenzyme TrxR. Further investigation revealed that **3** could induce ROS production and thiol depletion, and promote oxidative stress-mediated apoptosis in HL-60 cells. Clarification of the interaction of compound **3** with TrxR unveils the cellular target of the compound, and sheds light in considering development of it as a potential cancer chemotherapeutic agent.

4. Experimental section

4.1. Materials

The recombinant rat TrxR1 (WT TrxR1) was a gift from Prof. Arne Holmgren (Karolinska Institute, Sweden). The *E. coli* Trx and recombinant U498C TrxR1 mutant (Sec→Cys) were produced as described [12]. The shRNA plasmids targeting TrxR1 (shTrxR1) and non-targeting control (shNT), and HEK 293T cells stably transfected with a vector (HEK-IRES) and the cells stably overexpressing TrxR1 (HEK-TrxR1) were gifts from Prof. Constantinos Koumenis (University of Pennsylvania School of Medicine). All pictures of cell imaging were acquired by a FLoid Cell Imaging Station (Thermo Fisher Scientific). N-acetyl-L-cysteine (NAC), L-buthionine-(*S*, *R*)-sulfoximine (BSO), bovine insulin, N-acetyl-Asp-Glu-Val-Asp-p-nitroanilide (Ac-DEVD-pNA), G418, 3-[(3-Cholamidopropyl) dimethylammonio]-1-propanesulfonate (CHAPS), reduced glutathione (GSH), glutathione disulfide (GSSG), yeast glutathione reductase (GR), puromycin, dimethyl sulfoxide (DMSO), 2', 7'-dichlorfluorescein diacetate (DCFH-DA), Dulbecco's modified Eagle's medium (DMEM), RPMI 1640 medium and Hoechst 33342 were obtained from Sigma-Aldrich (St. Louis, USA). NADPH was purchased from Roche (Mannheim, Germany). Fetal bovine serum (FBS) was obtained from Sijiqing (Hangzhou, China). The PVDF membrane was from Millipore (Billerica, MA). Penicillin, streptomycin, and 3-(4, 5-Dimethylthiazol-2-yl)-2, 5-diphenyltetrazolium bromide (MTT) were obtained from Amresco (Solon, OH). Bovine serum albumin (BSA), sodium orthovanadate (V) (Na_3VO_4), trypan blue phenylmethylsulfonyl fluoride (PMSF), and actin antibody (AA128-1) were obtained from Beyotime (Nantong, China). The apoptosis detection kit containing propidium iodide (PI) and fluorescein-5-isothiocyanate-conjugated

Annexin V (Annexin V-FITC) was from Zoman Biotech (Beijing, China). DTNB was obtained from J&K Scientific (Beijing, China). TrxR1 primary antibody (sc-28321), anti-mouse IgG-HRP (sc-2031), anti-rabbit IgG-HRP (sc-2004) and dihydroethidium (DHE) were obtained from Santa Cruz Biotechnology (Santa Cruz, CA). ^{1}H NMR and ^{13}C NMR spectra were recorded with a Bruker AMX spectrometer at 400 and 100 MHz, respectively, using TMS as the internal standard. Mass spectra were recorded on Trace DSQ GC-MS spectrometer. All other reagents were of analytical grade and were purchased from commercial supplies. All reactions were carried out under a deoxygenated and dry argon atmosphere unless otherwise indicated.

*4.2. General method for the preparation of naphthazarin*s

To a mixture of anhydrous $AlCl_3$ (10 mmol, 1.33 g) and NaCl (5 mmol, 0.29 g) that was heated in an oil bath till molten was added maleic anhydride or 2-methylmaleic anhydride (1 mmol) and 1, 4-benzenediol or 4-chlorophenol (1 mmol). The temperature was slowly increased and maintained at 165 ^{o}C for 4 h. The reaction mixture was cooled to 0 ^{o}C, and 10 mL of 10% HCl was added, and the mixture was stirred for 15 min at 0 °C and then refluxed for 30 min. The reaction mixture was cooled to room temperature and extracted with ethyl acetate. The resulting product was purified by silica gel column chromatography using petroleum ether and ethyl acetate as the mobile phase. For preparation of substituted naphthazarins, compound **2** (114 mg, 0.6 mmol) was stirred in EtOH (10 mL), and different amines (0.7 mmol) were added. The reaction was allowed to stir for several hours at room temperature and the reaction process was monitored by thin layer chromatography. After the reaction completed, the solvent was evaporated under vacuum, and the resulting product was purified by silica gel column chromatography using petroleum ether and ethyl acetate as the mobile phase.

*4.2.1. 5-chloro-8-hydroxy-1, 4-naphthoquinone (**1**)*

Yield: 22%. ^{1}H NMR (400 MHz, $CDCl_3$): δ 12.62 (s, 1H), 7.64 (d, J = 8.8 Hz, 1H), 7.25 (d, J = 8.8 Hz, 1H), 6.95 (m, 2H). ^{13}C NMR (100 MHz, $CDCl_3$): δ 189.8, 182.7, 161.3, 140.9, 140.4, 136.9, 126.8, 126.4, 125.5, 116.0. EI-MS *m/z* (%): 208 (M^+, 100), 207 (32), 210(31), 152 (23), 57 (21), 71 (21), 126 (20), 85 (19), 44 (16).

*4.2.2. 5, 8-dihydroxy-1, 4-naphthoquinone (**2**)*

Yield: 15%. ^{1}H NMR (400 MHz, DMSO): δ 12.22 (s, 2H), 7.28 (s, 4H). ^{13}C NMR (100 MHz, DMSO): δ 172.2, 134.5. EI-MS *m/z* (%): 190 (M^+, 100), 189 (49).

*4.2.3. 2-methyl-5, 8-dihydroxy-1, 4-naphthoquinone (**3**)*

Yield: 20%. ^{1}H NMR (400 MHz, $CDCl_3$): δ 12.57 (s, 1H), 12.45 (s, 1H), 7.21 (m, 2H), 6.90 (s, 1H), 2.24 (s, 3H). ^{13}C NMR (100 MHz, $CDCl_3$): δ 183.3, 182.9, 162.9, 162.3, 148.2, 135.2, 131.2, 130.9, 111.8, 16.2. EI-MS *m/z* (%): 204 (M^+, 100), 189 (22).

*4.2.4. 2-methylamino-5, 8-dihydroxy-1, 4-naphthoquinone (**4**)*

Yield: 85%. ^{1}H NMR (400 MHz, DMSO): δ13.70 (s, 1H), 11.68 (s, 1H),8.09 (m, 1H), 7.32 (d, *J* = 9.2 Hz, 1H), 7.20 (d, *J* = 9.2 Hz, 1H), 5.60 (s, 1H), 2.84 (s, 3H).^{13}C NMR (100 MHz, DMSO): δ 186.1, 183.6, 156.3, 155.0, 150.6, 130.7, 125.7, 111.7, 111.1, 98.6, 29.2. EI-MS *m/z* (%): 219 (M^+, 100), 218 (23), 149(18).

*4.2.5. 2-ethylamino-5, 8-dihydroxy-1, 4-naphthoquinone (**5**)*

Yield: 89%. ^{1}H NMR (400 MHz, DMSO): δ13.71 (s, 1H), 11.69 (s, 1H), 8.01 (m, 1H), 7.32 (d, *J* = 9.2 Hz, 1H), 7.20 (d, *J* = 9.2 Hz, 1H), 5.68 (s, 1H), 3.28 (q, 2H), 1.18 (t, 3H).^{13}C NMR (100 MHz, DMSO): δ 186.1, 183.8, 156.3, 154.9, 149.4, 130.7, 125.6, 111.7, 111.0, 98.5, 36.9, 12.9. EI-MS *m/z* (%): 233 (M^+, 95), 218 (100).

*4.2.6. 2- propylamino-5, 8-dihydroxy-1, 4-naphthoquinone (**6**)*

Yield: 88%. ^{1}H NMR (400 MHz, DMSO): δ13.72 (s, 1H), 11.70 (s, 1H), 8.05 (m, 1H), 7.33 (d, *J* = 9.2 Hz, 1H), 7.20 (d, *J* = 9.2 Hz, 1H), 5.70 (s, 1H), 3.22 (t, 2H), 1.64 (m, 2H), 0.92 (t, 3H). ^{13}C NMR (100 MHz, DMSO): δ 186.1, 183.7, 156.3, 154.9, 149.7, 130.7, 125.6, 111.7, 111.0, 98.5, 43.7, 20.7, 11.3. EI-MS *m/z* (%): 247 (M^+, 47), 218 (100), 149 (25), 219 (21).

*4.2.7. 2-n-butylamino-5, 8-dihydroxy-1, 4-naphthoquinone (**7**)*

Yield: 85%. ^{1}H NMR (400 MHz, DMSO): δ13.71 (s, 1H), 11.70 (s, 1H), 8.03 (m, 1H), 7.32 (d, *J* = 9.2 Hz, 1H), 7.19 (d, *J* = 9.2 Hz, 1H), 5.67 (s, 1H), 3.24 (t, 2H), 1.58 (m, 2H), 1.36 (m, 2H), 0.92 (t, 3H).^{13}C NMR (100 MHz, DMSO): δ 186.1, 183.7, 156.3, 154.9, 149.6, 130.7, 125.6, 111.7, 111.0, 98.5, 41.8, 29.4, 19.6, 13.6. EI-MS *m/z* (%): 261 (M^+, 33), 44 (100), 218 (81), 57 (35), 149 (29), 194 (24).

*4.2.8. 2- n-hexylamino-5, 8-dihydroxy-1, 4-naphthoquinone (**8**)*

Yield: 87%. ^{1}H NMR (400 MHz, DMSO): δ13.71 (s, 1H), 11.69 (s, 1H), 8.03 (m, 1H), 7.32 (d, *J* = 9.2 Hz, 1H), 7.19 (d, *J* = 9.2 Hz, 1H), 5.67 (s, 1H), 3.21 (t, 2H), 1.58 (m, 12H), 1.28 (m, 10H), 0.86 (t, 3H). ^{13}C NMR (100 MHz, DMSO): δ 186.1, 183.7, 156.3, 154.9, 149.6, 130.7, 125.6, 111.7, 111.0, 98.5, 42.1, 31.2, 28.7, 28.6, 27.2, 26.4, 22.0, 13.9. EI-MS *m/z* (%): 317 (M^+, 33), 218 (100),

156 (24), 219 (23).

*4.2.9. 2-hydroxyethylamino-5, 8-dihydroxy-1, 4-naphthoquinone (**9**)*

Yield: 89%. ^{1}H NMR (400 MHz, DMSO): δ13.68 (s, 1H), 11.68 (s, 1H), 7.79 (m, 1H), 7.33 (d, *J* = 9.2 Hz, 1H), 7.21 (d, *J* = 9.2 Hz, 1H), 5.75 (s, 1H), 4.90 (m, 1H), 3.62 (m, 2H), 3.31 (m, 2H). ^{13}C NMR (100 MHz, DMSO): δ 186.3, 183.6, 156.3, 154.9, 149.9, 130.8, 125.7, 111.6, 110.9, 98.9, 58.4, 44.8. EI-MS *m/z* (%): 249 (M^+, 35), 218 (100), 219 (15).

*4.2.10. 2-isobutylamino -5, 8-dihydroxy-1, 4-naphthoquinone (**10**)*

Yield: 85%. ^{1}H NMR (400 MHz, DMSO): δ13.72 (s, 1H), 11.71 (s, 1H), 7.62 (m, 1H), 7.33 (d, *J* = 9.2 Hz, 1H), 7.20 (d, *J* = 9.2 Hz, 1H), 5.72 (s, 1H), 3.58 (m, 1H), 1.70 (m, 1H), 1.57 (m, 1H), 1.19 (d, *J* = 6.4 Hz, 2H), 0.89 (t, *J* = 7.2 Hz, 3H). ^{13}C NMR (100 MHz, DMSO): δ 186.1, 183.7, 156.2, 154.8, 148.9, 130.6, 125.5, 111.6, 110.8, 98.5, 49.5, 27.8, 18.7, 10.4. EI-MS *m/z* (%): 261 (M^+, 47), 232 (100), 71 (24), 57 (23), 85 (21).

*4.2.11. 2-isobutylamino-5, 8-dihydroxy-1, 4-naphthoquinone (**11**)*

Yield: 80%. ^{1}H NMR (400 MHz, DMSO): δ13.70 (s, 1H), 11.69 (s, 1H), 8.00 (m, 1H), 7.32 (d, *J* = 9.2 Hz, 1H), 7.19 (d, *J* = 9.2 Hz, 1H), 5.65 (s, 1H),3.25 (m, 2H), 1.67 (m, 1H),1.48 (m, 2H), 0.92 (d, *J* = 6.8 Hz, 6H). ^{13}C NMR (100 MHz, DMSO): δ 186.0, 183.7, 156.3, 154.9, 149.5, 130.7, 125.6, 111.7, 111.0, 98.5, 40.4, 35.9, 25.4, 22.3. EI-MS *m/z* (%): 275 (M^+, 36), 218 (100), 219 (54), 178 (19).

*4.2.12. 2-phenylamino-5, 8-dihydroxy-1, 4-naphthoquinone (**12**)*

Yield: 82%. ^{1}H NMR (400 MHz, DMSO): δ13.36 (s, 1H), 11.78 (s, 1H), 9.59 (s, 1H), 7.49 (m, 2H), 7.40 (m, 3H), 7.29 (m, 2H), 6.55 (s, 1H), 6.01 (s, 1H). ^{13}C NMR (100 MHz, DMSO): δ 187.2, 183.7, 156.4, 154.9, 149.7, 147.6, 137.6, 130.7, 129.4, 126.4, 125.9, 124.1, 115.6, 111.7, 110.9, 101.3. EI-MS *m/z* (%): 281 (M^+, 40), 149 (100), 45 (83).

*4.2.13. 2- phenylmethylamino-5, 8-dihydroxy-1, 4-naphthoquinone (**13**)*

Yield: 81%. ^{1}H NMR (400 MHz, DMSO): δ13.54 (s, 1H), 11.71 (s, 1H), 8.60 (m, 1H), 7.35 (m, 3H), 7.32 (d, *J* = 9.3 Hz, 1H), 7.28 (m, 1H), 7.21 (d, *J* = 9.3 Hz, 1H), 5.59 (s, 1H), 4.50 (d, *J* = 6.4 Hz, 1H). ^{13}C NMR (100 MHz, DMSO): δ 186.3, 183.7, 156.3, 155.0, 149.6, 137.0, 130.7, 128.5, 127.2, 127.1, 125.9, 111.7, 110.9, 99.8, 45.2. EI-MS *m/z* (%): 295 (M^+, 67), 91 (100), 129 (50), 204 (34).

*4.2.14. 2-piperidyl-5, 8-dihydroxy-1, 4-naphthoquinone (**14**)*

Yield: 89%. ^{1}H NMR (400 MHz, DMSO): δ13.35 (s, 1H), 11.70 (s, 1H), 7.30 (d, *J* = 9.2 Hz, 1H), 7.21 (d, *J* = 9.2 Hz, 1H), 6.00 (s, 1H), 3.57 (m, 4H), 1.65 (m, 6H). ^{13}C NMR (100 MHz, DMSO): δ 186.1, 185.3, 155.9, 154.5, 154.1, 129.2, 126.4, 113.4, 111.1, 108.4, 50.3, 25.5, 23.6. EI-MS *m/z* (%): 273 (M^+, 100), 149 (95), 43 (70), 57 (69), 83 (66).

*4.2.15. 2-morpholin-5, 8-dihydroxy-1, 4-naphthoquinone (**15**)*

Yield: 88%. ^{1}H NMR (400 MHz, DMSO): δ13.22 (s, 1H), 11.73 (s, 1H), 7.32 (d, *J* = 9.2 Hz, 1H), 7.24 (d, *J* = 9.2 Hz, 1H), 6.06 (s, 1H), 3.74 (m, 4H), 3.61 (m, 4H). ^{13}C NMR (100 MHz, DMSO): δ 186.7, 185.0, 156.1, 154.7, 154.0, 129.4, 126.8, 113.2, 111.0, 109.6, 65.7, 49.4. EI-MS *m/z* (%): 275 (M^+, 10), 149 (100), 167 (35), 57 (30).

*4.2.16. 2-(pyrrolidin-1-yl)-5, 8-dihydroxy-1, 4-naphthoquinone (**16**)*

Yield: 80%. ^{1}H NMR (400 MHz, DMSO): δ13.79 (s, 1H), 11.86 (s, 1H), 7.30 (d, *J* = 9.2 Hz, 1H), 7.19 (d, *J* = 9.2 Hz, 1H), 5.64 (s, 1H), 3.98 (m, 2H), 3.38 (m, 2H), 1.94 (m, 4H). ^{13}C NMR (100 MHz, DMSO): δ 185.5, 185.0, 156.1, 154.4, 149.5, 129.7, 125.6, 112.6, 111.1, 103.0. EI-MS *m/z* (%): 259 (M^+, 100), 190 (24), 149 (19).

4.3. Cell lines and culture conditions

HL-60, HepG2, HeLa, HEK 293T and L02 cells were obtained from the Shanghai Institute of Biochemistry and Cell Biology, Chinese Academy of Sciences. HepG2, HeLa, HEK 293T and L02 cells were kept in DMEM with 10% FBS, 2 mM glutamine, and 100 units/ml penicillin/streptomycin and maintained in an atmosphere of 5% CO_2 at 37 °C. HL-60 cells were kept in RPMI 1640 supplemented 10% FBS under the same conditions. HeLa-shNT and HeLa-shTrxR1 cells were generated in our lab [38] and were cultured under the same conditions as those of HeLa cells with additional supplement of puromycin (1 μg/ml) in DMEM. HEK-IRES and HEK-TrxR1 cells were cultured under the same conditions as those of HEK 293T cells with additional supplement of 0.1 μM sodium selenite and 0.4 mg/ml G418 in DMEM.

4.4. Cell viability analysis.

4.4.1. MTT assay

Cells (1×10^4) were incubated with compounds in triplicate in a 96-well plate for indicated times at 37 °C in a final volume of 100 μL. Controls were treated with 0.1% DMSO alone. At the end of

the treatment, 10 μl of MTT (5 mg/ml) was added and continued incubating for additional 4 h. After addition of the extraction buffer (100 μl, 10% SDS, 5% iso-butanol, 0.1% HCl), cells were further incubated overnight. The absorbance was determined at 570 nm using a microplate reader (Thermo Scientific Multiskan GO, Finland). Data are calculated as cell viability (% control) and corresponds to the percentage viable cells compared to untreated cells.

4.4.2. Trypan blue exclusion assay

HL-60 cells (5×10^4) were incubated with **3** or other agents in 24-well plates for indicated times at 37 °C. Controls were treated with DMSO alone, and cell viability was measured by the trypan blue exclusion assay. After treatment indicated times, the cells were stained with trypan blue (0.4%, w/v), and the number of dead (stained) and viable (non-stained) cells were determined using a microscope.

4.5. Purified TrxR activity assay

The purified TrxR activity was measured by the DTNB reduction assay. NADPH-reduced TrxR (85 nM) or U498C TrxR (350 nM) was incubated with varying concentrations of **3** for 1 h at room temperature in a 96-well plate (50 μL). A master mixture containing NADPH and DTNB in TE buffer (50 mM Tris-HCl, 1 mM EDTA, pH 7.5, 50 μL) was added. The final concentrations of DTNB and NADPH in the mixture are 2 mM and 200 μM, respectively. The linear increase of optical density at 412 nm from the initial 3 min was read. TrxR activity was expressed as percentage of the control.

4.6. GR assay

The NADPH-reduced GR (0.25 units/ml) in TE buffer was incubated with varying concentrations of **3** for 1 h in a 96-well plate at room temperature in a total volume of 100 μL. Reactions were initiated by the addition of NADPH (final concentration 400 μM) and GSSG (final concentration 1 mM). The GR activity was assayed by monitoring the decrease in absorbance at 340 nm during the initial 3 min. The GR activity was expressed as percentage of the control.

4.7. Imaging TrxR activity in HL-60 cells by TRFS-green

We employed TRFS-green, a specific fluorescence probe of TrxR, to image TrxR activity in

intact cells according to our published protocols [42]. Briefly, HL-60 cells (1×10^6) were incubated with indicated concentrations of **3** in 12-well plates for 8 h, then followed by further incubation with TRFS-green (10 μM) for 4h at 37 °C. The fluorescence and bright field images were acquired.

4.8. Assay of TrxR activity in cell lysates by the endpoint insulin reduction assay

HL-60 cells (70-80% confluence) were incubated with varying concentrations of **3** for 24 h. They were harvested, and washed twice with phosphate-buffered saline (PBS). Total cellular proteins were extracted by RIPA buffer (50 mM Tris-HCl pH 7.5, 0.5% deoxycholate, 2 mM EDTA, 0.1% SDS, 150 mM NaCl, 1% Triton X-100, 1 mM PMSF and 1 mM Na_3VO_4) for 30 min on ice, and were quantified using the Bradford procedure. TrxR activity in cell lysates was assayed by the endpoint insulin reduction assay according to our published protocols [41].

4.9. Measurement of ROS production

HL-60 cells (5×10^5) were plated in 12-well plates and were treated with the indicated concentrations of **3** for 1 h. The ROS indicator DHE (10 μM) or DCFH-DA (10 μM) in fresh FBS-free medium was added to each well, and further incubated for 30 min at 37 °C. The cells were viewed and images were acquired.

4.10. Measurement of intracellular thiols

After treatment of HL-60 cells (2×10^6) with increasing concentrations of **3** for 24 h in 100 mm dishes, the cells were collected, and washed twice with PBS. Total cellular proteins were extracted by RIPA buffer, and were quantified using the Bradford procedure. Total cellular thiols were measured by DTNB-titration. Briefly, cell lysate (10 μL) was added to cuvettes containing DTNB (1 mM in 90 μL of 6 M guanidine hydrochloride, pH 8.0). After incubation for 5 min at room temperature, the absorbance at 412 nm was read on a microplate reader. Total thiols were calculated from a calibration curve using GSH as the standard.

4.11. Measurement of cellular glutathiones

Measurement and quantification of the total glutathione and GSSG was based on the enzymatic recycling method according to our previously published [41]. Cells (2×10^6) were treated with the

indicated concentrations of **3** for 24 h in 100 mm dishes, and were resuspended using ice-cold extraction buffer containing 0.1% Triton X-100 and 0.6% sulfosalicyclic acid in 0.1 M potassium phosphate buffer with 5 mM EDTA, pH 7.5 (KPE buffer). After sonication of the suspension in ice water for 2-3 min with vortexing every 30 s, the solution was centrifuged at 3000 g for 4 min at 4 °C, and the supernatant was immediately collected. To assay the total glutathione, a solution (120 μl) containing 1.66 units/ml GR and 0.33 mg/ml DTNB was added to each sample (20 μl). Then NADPH (60 μl of 0.66 mg/ml) was added and the absorbance at 412 nm was immediately readed every 10 s for 2 min. GSSG was determined after GSH derivatization by 2-vinylpyridine. Briefly, two microliters of 2-vinylpyridine was added to 100 μl of cell supernatant and mixed, then the reaction was allowed to take place for 1 h at room temperature in a fume hood. Finally, six microliters of triethanolamine was added to the supernatant and the solution was mixed. Assay of GSSG was performed as described above for total glutathione. The amount of GSSG was subtracted from the total glutathione to give the GSH content.

4.12. Western blot analysis

For western blot analysis, total cellular proteins were extracted by RIPA buffer, and were quantified using the Bradford procedure. Equal amounts of protein in each lysate sample were separated by SDS-PAGE (12% gel, 40 μg per lane) under reducing conditions and then transferred to poly-vinylidene difluoride (PVDF) membranes (Millipore, USA). The blots were blocked with 5% non-fat milk in TBST at room temperature for 2 h, then membranes were incubated with specific primary antibodies in 5% non-fat milk at 4 °C overnight. Following three washes with TBST, the membranes were incubated with the peroxidase conjugated secondary antibodies for 1 h at room temperature. The immunoreactive bands were visualized by using an enhanced chemiluminescence kit from GE Healthcare.

4.13. Apoptosis assays

4.13.1. Assessment of caspase 3 activity

After treatment of HL-60 cells (2×10^6) with varying concentrations of **3** for 24 h in 100 mm dishes, the cells were collected, and washed twice with PBS. Total cellular proteins were extracted by RIPA buffer, and were quantified using the Bradford procedure. A cell extract containing 50 μg of

total proteins was incubated with the assay mixtures (50 mM Hepes, 0.1% CHAPS, 2 mM EDTA, 5% glycerol, 10 mM DTT, 0.2 mM Ac-DEVD-pNA, pH 7.5) for 2 h at 37 °C in a final volume of 100 μl. The absorbance at 405 nm was readed by using a microplate reader. Controls were treated with the same amounts of DMSO alone and the caspase 3 activity was expressed as the percentage of the control.

4.13.2. Annexin V/PI staining

HL-60 cells (1×10^6) were incubated with 0.5, 1, 3 and 5 μM **3** for 24 h in 6-well plates. The cells were harvested and washed twice with PBS. The apoptotic cells, necrotic cells and live cells were identified by the PI double and Annexin V-FITC staining assay according to the manufacturer's instructions. After staining, the cells were determined by a FACSCanto™ flow cytometer (BD Biosciences, USA), and the data were analyzed with the CellQuest software.

4.13.3. Hoechst 33342 staining

HL-60 cells (1×10^5) were plated in 12-well plates and incubated with 0.5, 1, 3 or 5 μM **3** for 24 h. Hoechst 33342 was added to reach a final concentration of 5 μg/ml and further incubated for 20 minutes. The cells were viewed and photographed.

4.14. Molecular docking simulation

A covalent docking was performed in the program Schrödinger Suite (Schrödinger, LLC: New York, NY, 2015) to investigate the binding mode of compound **3** and the enzyme. A rat TrxR1 structure (PDB code 3EAN [48], Chain A and B) was obtained from the Protein Data Bank and further prepared in the Protein Preparation Wizard module. The residue Sec498 in chain A was selected as the reactive residue involved in the Michael addition and also set as the centroid of the docking pocket. The default parameters were used in the docking simulation.

4.15. Statistics

All data were presented as mean ± SE from 3-5 different experiments. The differences between sets of data were assessed by the Students *t*-test. Compare means between control and treatment groups were performed by using one-way analysis of variance (ANOVA). A p value <0.05 was used as the criterion for statistical significance.

Acknowledgements

The financial supports from Natural Science Foundation of China (21572093, 21778028) and the Fundamental Research Funds for the Central Universities (lzujbky-2016-49) are greatly acknowledged. The authors also appreciate Prof. Arne Holmgren (Karolinska Institute, Sweden) for the recombinant rat TrxR1 and Prof. Constantinos Koumenis (University of Pennsylvania) for cells and shRNA plasmids.

Appendix A. Supplementary data

The following is the supplementary data related to this article:

Conflicts of interest

The authors confirm that there are no conflicts of interest.

ACCEPTED MANUSCRIPT

References

[1] D.F. Mahmood, A. Abderrazak, K. El Hadri, T. Simmet, M. Rouis, The thioredoxin system as a therapeutic target in human health and disease, Antioxid Redox Signal, 19 (2013) 1266-1303.

[2] J. Lu, A. Holmgren, The thioredoxin antioxidant system, Free Radic Biol Med, 66 (2014) 75-87.

[3] M. Benhar, Nitric oxide and the thioredoxin system: a complex interplay in redox regulation, Biochim Biophys Acta, 1850 (2015) 2476-2484.

[4] M. Berggren, A. Gallegos, J.R. Gasdaska, P.Y. Gasdaska, J. Warneke, G. Powis, Thioredoxin and thioredoxin reductase gene expression in human tumors and cell lines, and the effects of serum stimulation and hypoxia, Anticancer Res, 16 (1996) 3459-3466.

[5] K.F. Tonissen, Targeting the human thioredoxin system by diverse strategies to treat cancer and other pathologies, Recent Pat DNA Gene Seq, 1 (2007) 164-175.

[6] J. Hellfritsch, J. Kirsch, M. Schneider, T. Fluege, M. Wortmann, J. Frijhoff, M. Dagnell, T. Fey, I. Esposito, P. Kolle, K. Pogoda, J.P. Angeli, I. Ingold, P. Kuhlencordt, A. Ostman, U. Pohl, M. Conrad, H. Beck, Knockout of mitochondrial thioredoxin reductase stabilizes prolyl hydroxylase 2 and inhibits tumor growth and tumor-derived angiogenesis, Antioxid Redox Signal, 22 (2015) 938-950.

[7] M.H. Yoo, X.M. Xu, B.A. Carlson, V.N. Gladyshev, D.L. Hatfield, Thioredoxin reductase 1 deficiency reverses tumor phenotype and tumorigenicity of lung carcinoma cells, J Biol Chem, 281 (2006) 13005-13008.

[8] J. Zhang, X. Li, X. Han, R. Liu, J. Fang, Targeting the Thioredoxin System for Cancer Therapy, Trends Pharmacol Sci, 38 (2017) 794-808.

[9] H.L. Ng, S. Chen, E.H. Chew, W.K. Chui, Applying the designed multiple ligands approach to inhibit dihydrofolate reductase and thioredoxin reductase for anti-proliferative activity, Eur J Med Chem, 115 (2016) 63-74.

[10] Y.W. Liang, J. Zheng, X. Li, W. Zheng, T. Chen, Selenadiazole derivatives as potent thioredoxin reductase inhibitors that enhance the radiosensitivity of cancer cells, Eur J Med Chem, 84 (2014) 335-342.

[11] B. Zhang, D. Duan, C. Ge, J. Yao, Y. Liu, X. Li, J. Fang, Synthesis of xanthohumol analogues and discovery of potent thioredoxin reductase inhibitor as potential anticancer agent, J Med Chem, 58 (2015) 1795-1805.

[12] Y. Liu, D. Duan, J. Yao, B. Zhang, S. Peng, H. Ma, Y. Song, J. Fang, Dithiaarsanes induce oxidative stress-mediated apoptosis in HL-60 cells by selectively targeting thioredoxin reductase, J Med Chem, 57 (2014) 5203-5211.

[13] K.K. Kaminska, H.C. Bertrand, H. Tajima, W.C. Stafford, Q. Cheng, W. Chen, G. Wells, E.S. Arner, E.H. Chew, Indolin-2-one compounds targeting thioredoxin reductase as potential anticancer drug leads, Oncotarget, 7 (2016) 40233-40251.

[14] J. Zhang, J. Yao, S. Peng, X. Li, J. Fang, Securinine disturbs redox homeostasis and elicits oxidative stress-mediated apoptosis via targeting thioredoxin reductase, Biochim Biophys Acta, 1863 (2016) 129-138.

[15] D. Duan, B. Zhang, J. Yao, Y. Liu, J. Fang, Shikonin targets cytosolic thioredoxin reductase to induce ROS-mediated apoptosis in human promyelocytic leukemia HL-60 cells, Free Radic Biol Med, 70 (2014) 182-193.

[16] D. Duan, J. Zhang, J. Yao, Y. Liu, J. Fang, Targeting Thioredoxin Reductase by Parthenolide Contributes to Inducing Apoptosis of HeLa Cells, J Biol Chem, 291 (2016) 10021-10031.

[17] D.J. Newman, G.M. Cragg, Natural Products as Sources of New Drugs from 1981 to 2014, J Nat Prod, 79 (2016) 629-661.

[18] B.B. Mishra, V.K. Tiwari, Natural products: an evolving role in future drug discovery, Eur J Med Chem, 46 (2011) 4769-4807.

[19] F.E. Koehn, G.T. Carter, The evolving role of natural products in drug discovery, Nat Rev Drug Discov, 4 (2005) 206-220.

[20] T.J. McBride, J.J. Oleson, D. Woolf, The activity of streptonigrin against the Rauscher murine leukemia virus in vivo, Cancer Res, 26 (1966) 727-732.

[21] S.R. Keyes, R. Loomis, M.P. DiGiovanna, C.A. Pritsos, S. Rockwell, A.C. Sartorelli, Cytotoxicity and DNA crosslinks produced by mitomycin analogs in aerobic and hypoxic EMT6 cells, Cancer Commun, 3 (1991) 351-356.

[22] E. Reich, I.H. Goldberg, M. Rabinowitz, Structure-activity correlations of actinomycins and their derivatives, Nature, 196 (1962) 743-748.

[23] V.P. Papageorgiou, A.N. Assimopoulou, E.A. Couladouros, D. Hepworth, K.C. Nicolaou, The chemistry and biology of alkannin, shikonin, and related naphthazarin natural products, Angew Chem Int Edit, 38 (1999) 270-301.

[24] J.A. Kim, E.K. Lee, S.J. Park, N.D. Kim, D.H. Hyun, C.G. Lee, J.H. Lee, K.M. Yang, K. Heo, T.G. Son, Novel anti-cancer role of naphthazarin in human gastric cancer cells, Int J Oncol, 40 (2012) 157-162.

[25] B.R. Acharya, S. Bhattacharyya, D. Choudhury, G. Chakrabarti, The microtubule depolymerizing agent naphthazarin induces both apoptosis and autophagy in A549 lung cancer cells, Apoptosis, 16 (2011) 924-939.

[26] C.C. Shen, W.J. Syu, S.Y. Li, C.H. Lin, G.H. Lee, C.M. Sun, Antimicrobial activities of naphthazarins from Arnebia euchroma, J Nat Prod, 65 (2002) 1857-1862.

[27] K. Sasaki, H. Abe, F. Yoshizaki, In vitro antifungal activity of naphthoquinone derivatives, Biol Pharm Bull, 25 (2002) 669-670.

[28] Y. Kim, Y.J. You, B.Z. Ahn, Naphthazarin derivatives (VIII): Synthesis, inhibitory effect on DNA topoisomerase-I, and antiproliferative activity of 6-(1-acyloxyalkyl)-5,8-dimethoxy-1,4-naphthoquinones, Arch Pharm (Weinheim), 334 (2001) 318-322.

[29] G.Y. Song, Y. Kim, X.G. Zheng, Y.J. You, H. Cho, J.H. Chung, D.E. Sok, B.Z. Ahn, Naphthazarin derivatives (IV): synthesis, inhibition of DNA topoisomerase I and cytotoxicity of 2- or 6-acyl-5,8-dimethoxy-1, 4-naphthoquinones, Eur J Med Chem, 35 (2000) 291-298.

[30] G.Y. Song, X.G. Zheng, Y. Kim, Y.J. You, D.E. Sok, B.Z. Ahn, Naphthazarin derivatives (II): formation of glutathione conjugate, inhibition of DNA topoisomerase-I and cytotoxicity, Bioorg Med Chem Lett, 9 (1999) 2407-2412.

[31] A.C. Johansson, L. Norberg-Spaak, K. Roberg, Role of lysosomal cathepsins in naphthazarin- and Fas-induced apoptosis in oral squamous cell carcinoma cells, Acta Oto-Laryngol, 126 (2006) 70-81.

[32] L. Miseviciene, Z. Anusevicius, J. Sarlauskas, I.F. Sevrioukova, N. Cenas, Redox reactions of the FAD-containing apoptosis-inducing factor (AIF) with quinoidal xenobiotics: A mechanistic study, Arch Biochem Biophys, 512 (2011) 183-189.

[33] M.Y. Kim, S.J. Park, J.W. Shim, K. Yang, H.S. Kang, K. Heo, Naphthazarin enhances ionizing radiation-induced cell cycle arrest and apoptosis in human breast cancer cells, Int J Oncol, 46 (2015) 1659-1666.

[34] D.B. Bruce, A.J.S. Sorrie, R.H. Thomson, 489. Reactions in fused aluminium chloride–sodium chloride, J. Chem. Soc., 0 (1953) 2403-2406.

[35] V.K. Tandon, H.K. Maurya, M.K. Verma, R. Kumar, P.K. Shukla, 'On water' assisted synthesis and biological evaluation of nitrogen and sulfur containing hetero-1,4-naphthoquinones as potent antifungal and antibacterial agents, European Journal of Medicinal Chemistry, 45 (2010) 2418-2426.

[36] J.C. Lien, L.J. Huang, J.P. Wang, C.M. Teng, K.H. Lee, S.C. Kuo, Synthesis and antiplatelet, antiinflammatory, and antiallergic activities of 2-substituted 3-chloro-1,4-naphthoquinone derivatives, Bioorgan Med Chem, 5 (1997) 2111-2120.

[37] Y. Kumagai, Y. Shinkai, T. Miura, A.K. Cho, The Chemical Biology of Naphthoquinones and Its Environmental Implications, Annu Rev Pharmacol, 52 (2012) 221-247.

[38] J.Q. Xu, Q. Cheng, E.S.J. Arner, Details in the catalytic mechanism of mammalian thioredoxin reductase 1 revealed using point mutations and juglone-coupled enzyme activities, Free Radical Bio Med, 94 (2016) 110-120.

[39] R.E. Huber, R.S. Criddle, Comparison of the chemical properties of selenocysteine and selenocystine with their sulfur analogs, Arch Biochem Biophys, 122 (1967) 164-173.

[40] L. Johansson, G. Gafvelin, E.S. Arner, Selenocysteine in proteins-properties and biotechnological use, Biochim

Biophys Acta, 1726 (2005) 1-13.
[41] J. Zhang, Y. Li, D. Duan, J. Yao, K. Gao, J. Fang, Inhibition of thioredoxin reductase by alantolactone prompts oxidative stress-mediated apoptosis of HeLa cells, Biochem Pharmacol, 102 (2016) 34-44.
[42] L.W. Zhang, D.Z. Duan, Y.P. Liu, C.P. Ge, X.M. Cui, J.Y. Sun, J.G. Fang, Highly Selective Off-On Fluorescent Probe for Imaging Thioredoxin Reductase in Living Cells, J Am Chem Soc, 136 (2014) 226-233.
[43] S.E. Eriksson, S. Prast-Nielsen, E. Flaberg, L. Szekely, E.S. Arner, High levels of thioredoxin reductase 1 modulate drug-specific cytotoxic efficacy, Free Radic Biol Med, 47 (2009) 1661-1671.
[44] J. Fang, J. Lu, A. Holmgren, Thioredoxin reductase is irreversibly modified by curcumin: a novel molecular mechanism for its anticancer activity, J Biol Chem, 280 (2005) 25284-25290.
[45] B. Kalyanaraman, V. Darley-Usmar, K.J. Davies, P.A. Dennery, H.J. Forman, M.B. Grisham, G.E. Mann, K. Moore, L.J. Roberts, 2nd, H. Ischiropoulos, Measuring reactive oxygen and nitrogen species with fluorescent probes: challenges and limitations, Free Radic Biol Med, 52 (2012) 1-6.
[46] Y. Du, H. Zhang, J. Lu, A. Holmgren, Glutathione and glutaredoxin act as a backup of human thioredoxin reductase 1 to reduce thioredoxin 1 preventing cell death by aurothioglucose, J Biol Chem, 287 (2012) 38210-38219.
[47] D. Hanahan, R.A. Weinberg, Hallmarks of cancer: the next generation, Cell, 144 (2011) 646-674.
[48] Q. Cheng, T. Sandalova, Y. Lindqvist, E.S. Arner, Crystal structure and catalysis of the selenoprotein thioredoxin reductase 1, J Biol Chem, 284 (2009) 3998-4008.

ACCEPTED MANUSCRIPT

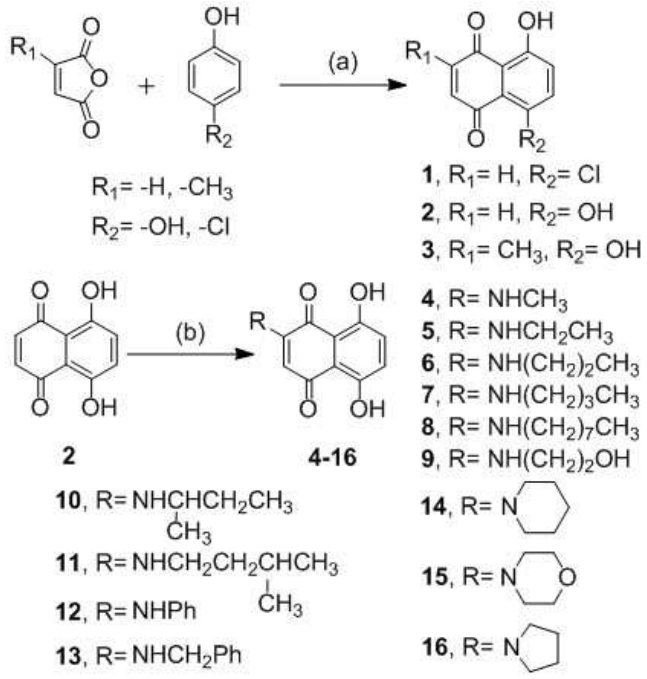

Scheme 1 Synthesis of compounds **1**-**16**. (a) 1) $AlCl_3$/NaCl, 165 °C for 4 h; 2) 10% HCl; (b) R-NH_2, EtOH, rt.

ACCEPTED MANUSCRIPT

668 **Table 1** Cytotoxicity of all compounds (**1-16**) against human promyelocytic leukemia HL-60 cells.

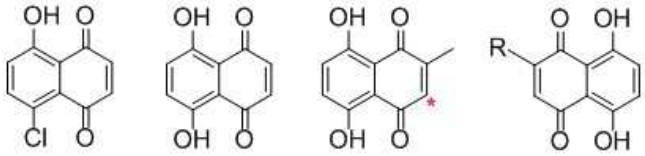

1 2 3 4-16

669

Compound	R substituents	Cell viability (%)*
1	—	23.08 ± 0.12
2	—	0
3	—	0
4	$NHCH_3$	62.96 ± 1.69
5	$NHCH_2CH_3$	56.39 ± 1.52
6	$NH(CH_2)_2CH_3$	59.38 ± 0.66
7	$NH(CH_2)_3CH_3$	59.21 ± 2.68
8	$NH(CH_2)_7CH_3$	61.10 ± 1.43
9	$NH(CH_2)_2OH$	50.28 ± 0.36
10	$NHCHCH_2CH_3$ CH_3	57.04 ± 2.16
11	$NHCH_2CH_2CHCH_3$ CH_3	54.26 ± 1.92
12	NHPh	59.72 ± 2.98
13	$NHCH_2Ph$	54.58 ± 1.65
14		54.85 ± 1.28
15	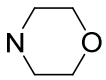	50.13 ± 3.29
16		97.23 ± 2.21

670 * Cells were treated with the tested compounds (20 μM) for 48 h and the cell viability was

671 determined by the MTT assay.

672

ACCEPTED MANUSCRIPT

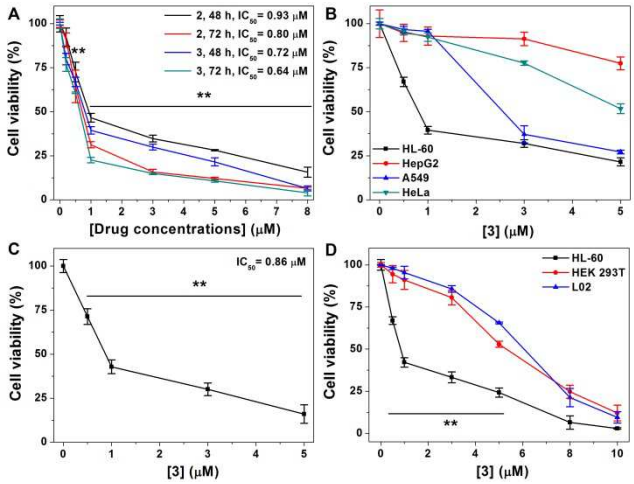

673

674 **Fig. 1** Cytotoxicity of compounds **2** and **3** in cells. (A) Time-dependent cytotoxicity of **2** or **3**
675 towards HL-60 cells. The HL-60 cells were incubated with the varying concentrations of **2** or **3** for
676 the indicated times. Cell viability was assessed by the MTT method. (B) Cytotoxicity of **3** towards
677 HL-60, A549, HepG 2, and HeLa cells. The cells were incubated with the indicated concentrations of
678 **3** for 48 h and the cell viability was assessed by the MTT method. (C) Cytotoxicity of **3** towards
679 HL-60 for 48 h. Cell viability was determined by the trypan blue exclusion assay. (D) Cytotoxicity of
680 **3** towards L02 and HEK 293T cells in comparison with HL-60 cells. Cells were treated with the
681 compound for 48 h, and the cell viability was assessed by the MTT method. Data are expressed as
682 mean ± SE from triplicates. **, P< 0.01 vs. the control groups in (A) & (C); **, P< 0.01 vs. the
683 normal cells in (D).

684

ACCEPTED MANUSCRIPT

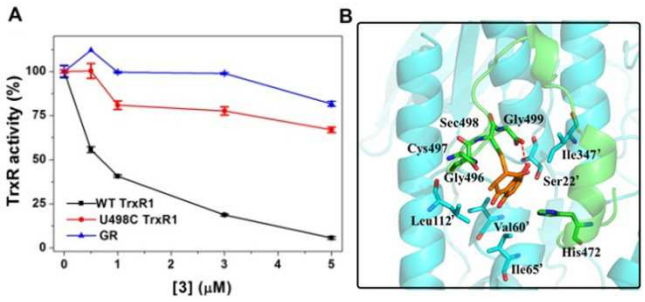

685

686 **Fig. 2** Targeting the Sec residue of TrxR by **3**. (A) Inhibition of purified TrxR, U498C TrxR and GR
687 by **3**. NADPH-reduced recombinant rat TrxR1 (WT TrxR1), U498C TrxR1, and GR were incubated
688 with the indicated concentrations of **3** for 1 h at room temperature, and the enzymes' activity was
689 determined and expressed as the percentage of the control. (B) Molecular docking of compound **3**
690 with TrxR1 was carried out using the covalent docking protocol in the program Schrödinger Suite
691 (Schrödinger, LLC: New York, NY, 2015). The docking score for the non-bonding interaction was
692 -5.81 kcal/mol. Two subunits of TrxR1 were represented by green and cyan cartoons respectively.
693

ACCEPTED MANUSCRIPT

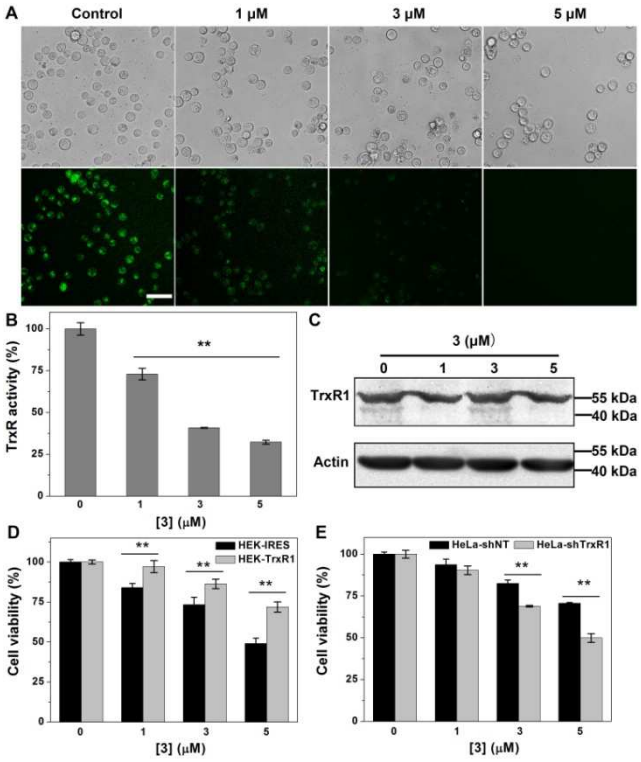

Fig. 3 Involvement of TrxR for the cellular action of **3**. (A) Imaging the cellular TrxR activity in live HL-60 cells by TRFS-green. After treatment of HL-60 cells with varying concentrations of **3** for 12 h, the TrxR activity was stained by the TrxR probe TRFS-green. The bright filed pictures (top panel) and the fluorescence pictures (bottom panel) were acquired. Scale bars: 20 μm. (B) Inhibition of TrxR activity in HL-60 cells by **3**. After the cells were treated with the indicated concentrations of **3** for 24 h, the TrxR activity in cells was determined by the end point insulin reduction assay. (C) No obvious changes of TrxR1 protein levels in HL-60 cells treated with **3**. Cells were treated with the indicated concentrations of **3** for 24 h, and the cell extracts were assessed by Western blots. (D) Overexpression of TrxR1 decreases the cytotoxicity of **3**. The HEK-IRES and HEK-TrxR1 cells were incubated with the various concentrations of **3** for 48 h, and the cell viability was assayed by the MTT method. (E) Knockdown of TrxR1 increases the cytotoxicity of **3**. The HeLa-shTrxR1and HeLa-shNT cells were incubated with the indicated concentrations of **3** for 48 h, and the cell viability was assayed by the MTT method. Data are expressed as mean ± SE of three experiments. **, $P< 0.01$ vs. the control groups in (B); **, $P< 0.01$ vs. the HEK-IRES cells in (D) and HeLa-shNT cells in (E).

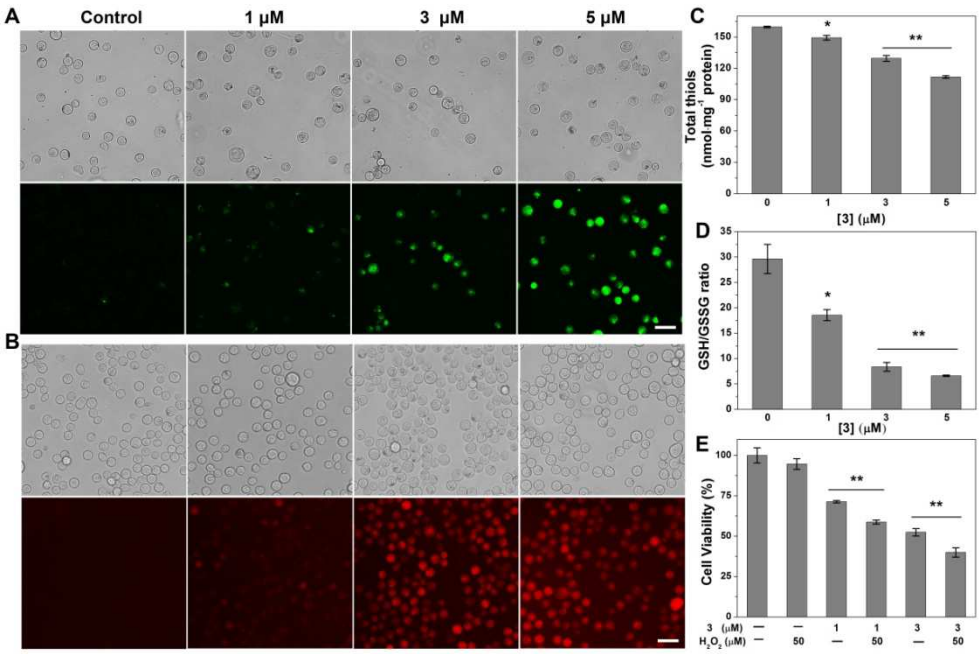

Fig. 4 Induction of oxidative stress by **3** in HL-60 cells. ROS accumulation in HL-60 cells determined by (A) DCFH-DA or (B) DHE staining. HL-60 cells were treated with varying concentrations of **3** for 1 h followed by the incubation with DCFH-DA (10 μM) or DHE (10 μM) for 30 min. The fluorescence pictures (bottom panel) and the bright filed pictures (top panel) were acquired. Scale bars: 20 μm. (C) Alteration of cellular total thiol levels after **3** treatment. HL-60 cells were treated with 1, 3 and 5 μM **3** for 24 h, and cellular total thiols were determined by DTNB titration. (D) Alteration of GSH/GSSG ratio in cells. The HL-60 cells were treated with **3** for 24 h. Intracellular GSH and GSSG levels were measured by enzymatic recycling method, and the GSH/GSSG ratio was shown. (E) Increase of hydrogen peroxide cytotoxicity by **3**. After treatment of HL-60 cells with 1 or 3 μM **3** in the absence or presence of 50 μM hydrogen peroxide for 24 h, the cell viability was measured by the MTT assay. Data are expressed as mean ± SE from triplicates. *, $P < 0.05$ and **, $P < 0.01$ vs. the control groups in (C) and (D); **, $P < 0.01$ vs. the **3** groups in (E).

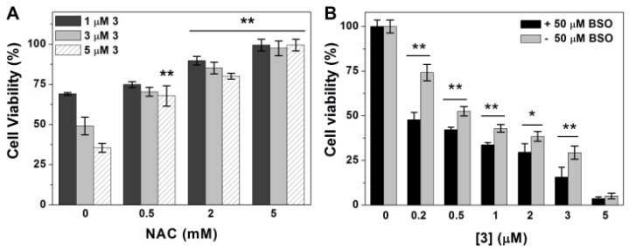

Fig. 5 Effect of NAC supplement and GSH depletion on the cytotoxicity of **3**. (A) Impairment of the cytotoxicity of **3** by NAC. After treatment of HL-60 cells with the indicated concentrations of NAC and **3** for 24 h, the cell viability was measured by the MTT assay. (B) Enhancement of the cytotoxicity of **3** by GSH depletion. HL-60 cells were incubated with 50 μM BSO for 24 h to reduce the intracellular GSH level, followed by **3** treatment for an additional 48 h, and the cell viability was measured by the MTT assay. Data are expressed as mean ± SE of three experiments. **, $P < 0.01$ vs. the groups without NAC in (A); *, $P < 0.05$ and **, $P < 0.01$ vs. the groups without BSO in (B).

ACCEPTED MANUSCRIPT

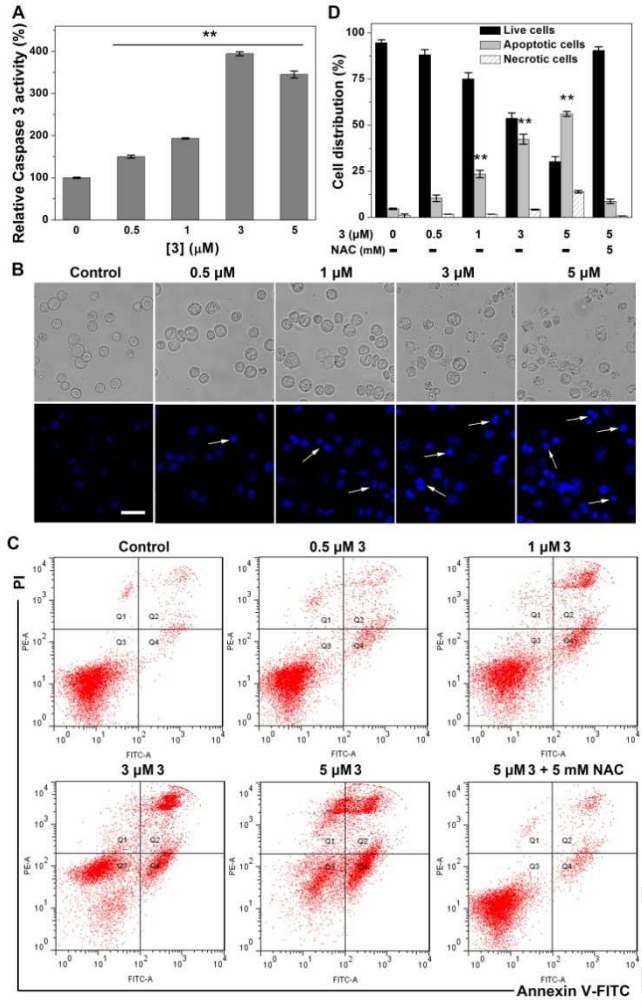

Fig. 6 Induction of apoptosis by **3** in HL-60 cells. (A) Activation of caspase 3 by **3** in HL-60 cells. HL-60 cells were treated with the indicated concentrations of **3** for 24 h and the caspase 3 activity in cell lysates was determined by a colorimetric assay. (B) Morphological and nuclear changes after **3** -treatment. HL-60 cells were treated with indicated concentrations of **3** for 24 h followed by Hoechst 33342 staining. Phase contrast (top panel) and fluorescence (bottom panel) images were acquired. Scale bars: 20 μm. (C) Analysis of apoptosis by Annexin V/PI double staining assay. HL-60 cells were treated with different concentrations of **3** for 24 h, and the population of live cells, apoptotic cells and necrotic cells was analyzed by flow cytometry. Cells in the scattergrams show four different cell populations marked as the follows: PI-positively and FITC-negatively stained cells showing necrotic cells (upper left, Q1), double-negative (unstained) cells showing live cells (lower left, Q3), FITC and PI double-stained cells showing late apoptosis (upper right, Q2), and FITC-positively and PI-negatively stained cells showing early apoptosis (lower right, Q4). (C) Quantification of live cells (Q3), apoptotic cells (Q2 and Q4), and necrotic cells (Q1) was illustrated. The data are expressed as

747 mean ± SE of three independent samples. P< 0.01 vs. the control groups in (A) and (D).

ACCEPTED MANUSCRIPT

ACCEPTED MANUSCRIPT

Highlights

► A panel of naphthazarin derivatives were synthesized.

► Compound **3** (2-methylnaphthazarin) shows highest cytotoxicity to HL-60 cells.

► Compound **3** inhibits thioredoxin reductase (TrxR).

► Overexpression of TrxR confers protection, while knockdown of TrxR increases toxicity of **3**.

► Compound **3** induces oxidative stress-mediated apoptosis of HL-60 cells.

ACCEPTED MANUSCRIPT